

# Universal building block for (110)-family silicon and germanium surfaces

Ruslan Zhachuk<sup>1,\*</sup> and Alexander Shklyaev<sup>1,2</sup>

<sup>1</sup>*Institute of Semiconductor Physics, pr. Lavrentyeva 13, Novosibirsk 630090, Russia*

<sup>2</sup>*Novosibirsk State University, ul. Pirogova 1, Novosibirsk 630090, Russia*

(Dated: January 3, 2020)

The universal building block which is an essential part of all atomic structures on (110) silicon and germanium surfaces and their vicinals is proposed by combining first-principles calculations and scanning tunneling microscopy (STM). The atomic models for the (110)–(16×2), (110)–*c*(8×10), (110)–(5×8) and (17151)–(2×1) surface reconstructions are developed on the basis of the building block structure. The models exhibit very low surface energies and excellent agreements with bias-dependent STM images. It is shown that the Si(47357) surface shares the same building block. Our study closes the long-debated pentagon structures on (110) silicon and germanium surfaces.

Over the past three decades, large efforts have been made to understand the atomic and electronic structure of (110) silicon and germanium surfaces using scanning tunneling microscopy (STM) and spectroscopy, photoelectron spectroscopy and first principles calculations [1–20]. This indicates both the complexity of the task and its high scientific relevance. One of the reasons for the persistent interest to these surfaces is their peculiar properties, such as high hole mobility in the devices fabricated on the Si(110) surface [21] and strong surface anisotropy. The second feature became especially attractive due to the recent success in the formation of single-domain (16×2) reconstruction on the Si(110) surface [22, 23]. This makes (110) surfaces very convenient substrates for the growth of one-dimensional objects, such as nanowires [24–29]. It is also worth noting that, among all low-index silicon and germanium surfaces, (100), (111) and (110) [Fig. 1(a)], only the (110) structure is still not understood, and, therefore, it is of significant academic interest as well.

The common feature of all reconstructed (110) silicon and germanium surfaces is the presence of bright spots exhibiting pentagonal or tetragonal shapes (hereafter polygons) in high-resolution STM images depending on acquisition conditions [4, 11]. When the Ge(110) surface is observed at an elevated temperature (above 430°C), the polygons are closely packed and show no long range order [8, 14, 30]. However, when the temperature is lowered to about 380°C the polygons begin to line up and their density is lowered, indicating the formation of the *c*(8×10) reconstruction. A very long annealing at 380°C converts the *c*(8×10) reconstruction into the (16×2) surface structure. Thus, the (16×2) reconstruction is equilibrium, while the *c*(8×10) surface structure is only a transient (metastable) structure of the Ge(110) surface. The structural transformations on the Si(110) surface are similar to those of the Ge(110) surface, but the transient structure is (5×8) [16]. The formation of polygons in varied experimental conditions at various temperatures is a strong indication of their exceptional stability owing to low formation energy values.

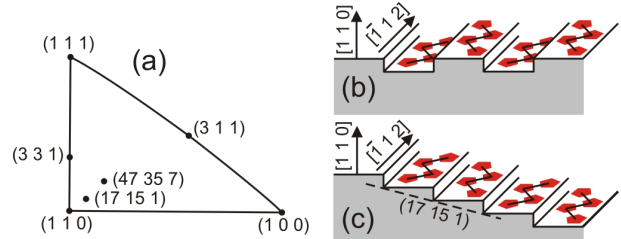


Figure 1. (a) Unit stereographic triangle with some stable silicon planes marked. (b), (c) Schematic views of (110)–(16×2) (b) and (17151)–(2×1) (c) silicon and germanium surfaces.

Perhaps, the most widely known structure of (110) silicon and germanium surfaces is the structure referred to as (16×2). This notation, however, does not follow the Wood’s notation [31], since this surface reconstruction can only be correctly described by a matrix [32]. According to the STM data, the (110)–(16×2) surface is composed of a periodic up-and-down sequence of terraces with the height difference equal to a single (110) atomic layer and ≈ 25 Å step-step separation [Fig. 1(b)]. The terraces exhibit the zig-zag chains of polygons along step edges. Thus, the structure appears as the equidistant stripes running in  $\langle \bar{1}12 \rangle$  directions and forming a natural substrate for the nanowire growth. Since the (16×2) reconstruction is an equilibrium structure of (110) silicon and germanium surfaces, it should provide a minimum free surface energy. Considering that the (110) terraces in the (16×2) reconstruction are relatively wide, the step-step interactions should be small and each step could be considered independently in the first approximation. Taking this note into account, the reconstructed (110) terraces, linked in a manner of “down, down, down, ...” [Fig. 1(c), or “up, up, up ...”] should also provide a free energy minimum and, therefore, be observed in experiments. A simple calculation shows that these surfaces would have {17151} orientations [4.4° off from the (110) plane, Figs. 1(a) and (c)]. Indeed, small facet planes of the {17151} orientation were found on (110) silicon

and germanium surfaces [1, 8, 14, 15, 33, 34]. Therefore, there is a tight structural relationship between the  $(17\ 15\ 1)-(2\times 1)$  and  $(110)-(16\times 2)$  surfaces. Since these surfaces are built from the same structural elements, they should have very close formation energies and electronic structures.

Thirteen full and partial atomic models were proposed to explain the structures found on  $(110)$  silicon and germanium surfaces [1–12, 35]. While there is a general consensus about the positioning of polygons in different surface reconstructions, the main difficulty is the atomic structure of the polygon itself. In this Letter we develop a realistic model of the building block which appears as polygons in the STM images of  $(110)$  silicon and germanium surfaces and their vicinals. Using this block we built the microscopic models of the  $(16\times 2)$ ,  $c(8\times 10)$  and  $(5\times 8)$  reconstructions of the  $(110)$  surfaces which show a remarkably low surface energy and closely reproduce the experimental bias-dependent STM images. We demonstrate that the vicinal  $(110)$  surfaces, such as  $(17\ 15\ 1)$  and  $(47\ 35\ 7)$ , also share the same universal building block.

The calculations were carried out using the pseudopotential [36] density functional theory SIESTA code [37] within the local density approximation (LDA) to the exchange and correlation interactions between electrons [38]. The valence states were expressed as linear combinations of the Sankey-Niklewski-type numerical atomic orbitals [37]. In the present calculations, the polarized double- $\zeta$  functions were assigned for all species. This means two sets of  $s$ - and  $p$ -orbitals plus one set of  $d$ -orbitals on silicon and germanium atoms, and two sets of  $s$ -orbitals plus a set of  $p$ -orbitals on hydrogen atoms. The electron density and potential terms were calculated on a real space grid with the spacing equivalent to a plane-wave cut-off of 200 Ry.

Following the other authors [5, 12], we neglect the contribution of entropy to the surface free energy and evaluate only the leading term (surface formation energy). In this work, we calculate the surface energy gain ( $\Delta\gamma$ ), due to the reconstruction and relaxation, with respect to the bulk-terminated  $(110)$  silicon and germanium surfaces [39].  $\Delta\gamma$  values were calculated using 6 layers thick slabs (7 layer slabs for the  $(16\times 2)$  reconstruction) terminated by hydrogen from one side. A 18 Å thick vacuum layer was used. We used specific  $\mathbf{k}$ -point grids for each surface reconstruction/slab, depending on its respective lateral dimensions, namely:  $2\times 2\times 1$  for  $(110)-(5\times 8)$  and  $c(8\times 10)$ ,  $1\times 4\times 1$  for  $(110)-(16\times 2)$ , and  $2\times 4\times 1$  for  $(17\ 15\ 1)-(2\times 1)$  [40]. The geometry was optimized until all atomic forces became less than 0.01 eV/Å. For the calculations of silicon and germanium chemical potentials we used the respective bulk supercells (with equilibrium lattice constants  $a_{Si} = 5.420$  Å and  $a_{Ge} = 5.650$  Å) with the lateral dimensions and  $\mathbf{k}$ -point grids identical to those used for slab calculations. The

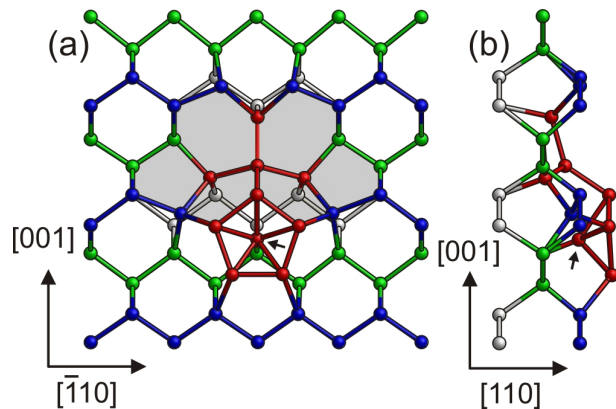


Figure 2. Universal building block (UBB) structure of reconstructed  $(110)$  silicon and germanium surfaces. The zig-zag atom chains in the  $[\bar{1}10]$  direction are the atoms of the first, second and third layers marked in blue, green and white, respectively. The additional atoms and atoms strongly shifted from their ideal  $(110)$  lattice positions are red. The interstitial atoms are highlighted by arrows. (a) Top view. The rebonded area is shaded. (b) Side view.

constant-current STM images were produced based on the Tersoff-Hamann approximation [41] using the eigenvalues and eigenfunctions of the Kohn-Sham equation [42] for a relaxed atomic structure. The surface optimized basis set (cut-off radii for  $s$ -,  $p$ -, and  $d$ -orbitals are  $R_s = 9$  Bohr,  $R_{pd} = 11$  Bohr for Si) was used for STM image calculations [43].

The STM images were recorded at room temperature in the constant-current mode using an electrochemically etched tungsten tip. The measurements were performed in an ultrahigh vacuum chamber ( $7\times 10^{-11}$  Torr) on a system equipped with an STM (OMICRON). A clean Si(47357) surface was prepared by the sample flash annealing at 1250 °C for 1 min followed by a stepwise cooling with an average rate of  $\approx 5$  °C/min within a temperature range from about 850 to 400 °C. The WSxM software was used to process the experimental and calculated STM images [44].

The structure of universal building block (UBB), proposed in this Letter, is shown in Figs. 2(a) and 2(b). It has the mirror symmetry with respect to the  $(\bar{1}10)$  plane. The UBB consists of the interstitial atom, which holds together five atoms of the surrounding pentamer, and closely integrated rebonded area [shaded area in Fig. 2(a)]. The pentamers with interstitial atoms were successfully applied to develop the atomic models of reconstructed Si(113) and Si(331) surfaces [45, 46]. Unfortunately, porting this structural unit to other surfaces is not straightforward, since these surfaces have different bond configurations. The rebonded area contains four pentagonal rings and two hexagonal rings [shaded area in Fig. 2(a)]. The UBB structure eliminates 8 dangling bonds on the unreconstructed  $(110)$  surface and requires

a very little mass transfer to be built, since each UBB contains only 3 additional atoms.

In Fig. 3(a) are the UBB model of the  $(17\ 15\ 1) - (2 \times 1)$  surface and the corresponding calculated constant-current STM image. The pentamer spots are labeled P1-P5 according to Ref. 11. The model illustrates both the arrangement of pentamers on  $(1\ 1\ 0)$  terraces and the step edge structure on  $(17\ 15\ 1) - (2 \times 1)$  and  $(1\ 1\ 0) - (16 \times 2)$  surfaces. The step edge structure shown in Fig. 3(a) is different from the structure proposed in Ref. 10. See Supplemental Material [URL will be inserted by publisher] for UBB models and the corresponding calculated STM images of  $(16 \times 2)$ ,  $c(8 \times 10)$  and  $(5 \times 8)$  reconstructions on the  $(1\ 1\ 0)$  surface. We note here that the UBB has a 3D structure, which is only partially accessible for STM observations. The interstitial atoms, as well as the re-bonded area atoms, are difficult to visualize, since all their bonds are saturated and they are located somewhat below the surface level. The visible pentamer size in the calculated STM image in Fig. 3(a) is larger than that from the atomistic model. The same statement holds for the experimental STM images. This size mismatch sustained an argument against the atomic models based on pentamers with interstitial atoms in the past [47]. The seeming disagreement, however, is explained by the presence of polarized surface radical states showing a pronounced angle with respect to the surface normal [43, 48, 49].

The constant-current STM images of pentamer pairs, outlined by the black square in Fig. 3(a), were calculated for the empty/filled electronic states and for low/moderate applied voltage to compare them with the available experimental data. The pentamers exhibit four lobes when observed using filled electronic states and five lobes when empty electronic states are used at the 1.0 V applied bias [Figs. 3(d) and (e)] in agreement with the experimental data [4, 11]. At the low bias (0.1 V), however, the pentamers show only four lobes at both polarities [Figs. 3(b) and (c)]. Again, this is in a full agreement with the experimental STM images reported in Ref. 11. The detailed inspection of the STM image in Fig. 3(e) reveals that the spots P1 and P2 facing the neighboring pentamer are brighter than other spots (P3-P5). Splitting the four-lobe pattern into five-lobes at the positive bias and increased intensity of P1 and P2 spots is caused by the empty state superposition at about 0.5 eV, as it was experimentally demonstrated by Setvín *et al.* [11]. Note that both shape and relative intensities of electronic states are very sensitive to the atomic structure and the UBB model reproduces them very well, while other models fail to describe even basic pentamers geometry. This is a strong argument for the validity of UBB model. Another argument is very low formation energy values for all surface structures composed of UBBs, as shown below.

Since many atomic models of the  $(1\ 1\ 0)$  surface structures have been proposed, we will compare our  $(1\ 1\ 0) -$

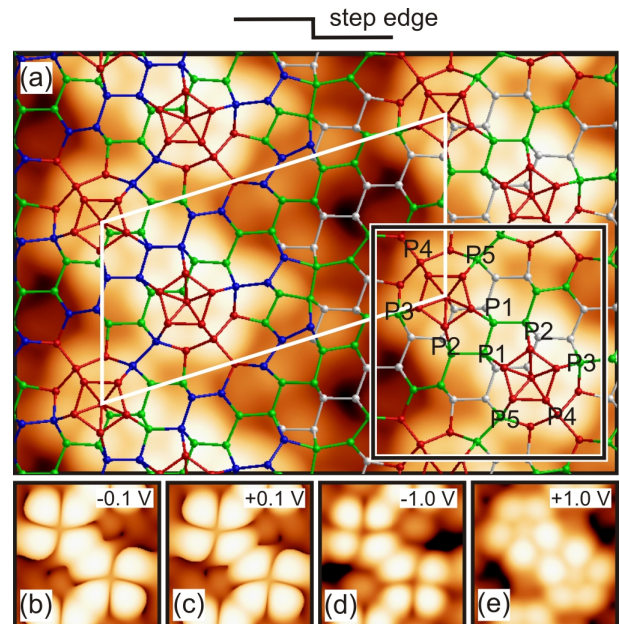


Figure 3. (a) UBB model of the  $\text{Si}(17\ 15\ 1) - (2 \times 1)$  surface and the corresponding calculated constant-current STM image assuming  $U = +1.0\ \text{V}$ . Zig-zag atom chains are the atoms in the  $[110]$  direction of the first three  $(1\ 1\ 0)$  layers marked in blue, green and white. The UBBs atoms are marked in red. The step edge (vertical) direction is  $[\bar{1}12]$ . The pentamer pairs are highlighted by a black square, the unit cell is shown by a white parallelogram. The pentamer spots are labeled P1-P5 according to Ref. 11. (b)-(e) The STM images of pentamer pairs on the  $\text{Si}(17\ 15\ 1) - (2 \times 1)$  surface calculated assuming different applied voltages.

Table I. Reconstruction-induced energy gain ( $\Delta\gamma$ ,  $\text{meV}/\text{\AA}^2$ ) for different models of the  $\text{Si}(1\ 1\ 0) - (16 \times 2)$  reconstruction with respect to the bulk-terminated  $\text{Si}(1\ 1\ 0)$  surface: ATI [5], THTR stepped [12] and UBB.

Model	$\Delta\gamma$
ATI	21.4, 21.6 [12], 23.8 [5]
THTR stepped	32.0, 30.5 [12]
UBB	31.5

$(16 \times 2)$  UBB model only with two other models: the adatom-tetramer-interstitial (ATI) model, the most cited in the literature [5] and the recently proposed tetramer heptagonal- and tetragonal-ring (THTR) stepped structure [12]. In Table I are the energy gains for three different  $(16 \times 2)$  reconstruction models. The ATI model by Stekolnikov *et al.* can be ruled out since it shows the low energy gain. In addition, the respective calculated constant-current STM images do not match the experimental STM images of  $\text{Si}(1\ 1\ 0) - (16 \times 2)$ , although the ATI model also contains pentamers with interstitial atoms. According to our calculations, the recently proposed THTR stepped model is slightly favored over

Table II. Number of UBBs per  $(110) - (1 \times 1)$  cell ( $n$ ), excess coverage ( $\Delta\theta$ , monolayers) and reconstruction-induced energy gain ( $\Delta\gamma$ ,  $\text{meV}/\text{\AA}^2$ ) with respect to the bulk-terminated  $(110)$  surface for various UBB-based structural models.

Reconstruction	$n$	$\Delta\theta$	$\Delta\gamma$	
			Si	Ge
$(16 \times 2)$	0.125	0.66	31.5	28.2
$(5 \times 8)$	0.1	0.15	30.4	28.1
$c(8 \times 10)$	0.1	0.15	30.2	28.1

UBB, when using LDA to the exchange and correlation interactions [Tab. I] [38], but the opposite trend is observed when the generalized gradient approximation (GGA) [50] is used. Anyway, the energy difference between THTR stepped and UBB models is within the typical error of about  $1 \text{ meV}/\text{\AA}^2$  for these type of calculations. Finally, we cannot exclude that the step edges on the  $(110) - (16 \times 2)$  surface have another atomic configuration than the one shown in Fig. 3(a). The THTR stepped model has a serious flaw, since the static model is incompatible with the experimental STM images of pentamers [12]. It was suggested that the model can reproduce STM images only when the dynamic buckling of reconstruction elements at room temperature is considered. There are two objections for this hypothesis. First, there is no indication that the pentamers at  $T = 78 \text{ K}$  look different than that at room temperature in the low-temperature STM study by Setvın *et al.* [11]. In fact, the pentamers look basically the same both in low- and in room-temperature STM images [51]. Second, the calculated constant-current STM images, averaged using two buckled surface configurations, do not reproduce the experimental STM images of pentamers as well (see Supplemental Material [*URL will be inserted by publisher*] for the calculated STM images of the ATI and THTR stepped models of  $\text{Si}(110) - (16 \times 2)$ ).

In table II is the number of UBBs per  $(110) - (1 \times 1)$  cell, excess coverage and reconstruction-induced energy gain with respect to the bulk-terminated  $(110)$  surface for various UBB-based structural models. All atomic structures show noticeably large energy gains, while the gain for  $(16 \times 2)$  structure is slightly higher than that for other two reconstructions. This is in agreement with the experimental results indicating that this structure is equilibrium [8, 14, 16, 30]. There is a correlation between the highest energy gain and the highest surface density of UBBs in the  $(16 \times 2)$  structure [Tab. II]. This finding can be interpreted in the way that the main physical reason for the low energy of reconstructed  $(110)$  surfaces is the presence of UBBs. Further, the formation of  $(5 \times 8)$  and  $c(8 \times 10)$  structures requires a very little mass transfer (addition of 0.15 monolayers), since it solely depends on the UBBs assembly. The  $(16 \times 2)$  structure requires a larger mass transfer (addition of 0.66 or removal of 0.34

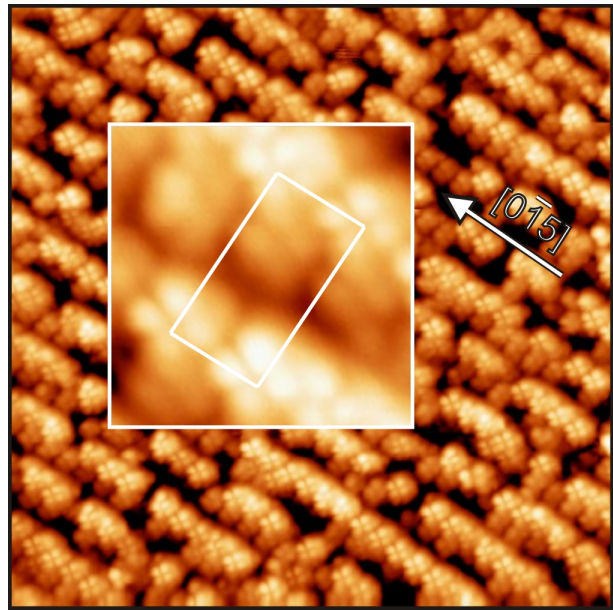


Figure 4. Experimental STM image of the  $\text{Si}(47\ 35\ 7)$  surface,  $400 \times 400 \text{\AA}^2$ .  $U = -0.8 \text{ V}$ ,  $I = 2.0 \text{ pA}$ . In the inset is a high-resolution STM image of the structure with the unit cell outlined,  $5 \times 5 \text{\AA}^2$ .

monolayers), since, in addition, it involves the formation of up and down steps. This observation clarifies the nature of metastable  $(5 \times 8)$  and  $c(8 \times 10)$  structures; namely, it shows that these structures are formed due to a limited mobility of surface atoms. A similar formation of metastable surface structures after rapid sample cooling was observed on the  $\text{Si}(111)$  surface [52, 53].

Finally, in Fig. 4, we show the experimental STM image of the stable  $\text{Si}(47\ 35\ 7)$  surface. This vicinal  $\text{Si}(110)$  surface, inclined at about  $10.7^\circ$  degrees to the  $(110)$  plane [Fig. 1(a)] was first observed and identified by Olshanetsky and Shklyaev using low-energy electron diffraction [54]. The STM image reveals the ordered reconstructed surface with the structural blocks aligned into straight chains along the  $[0\bar{1}5]$  direction. The high resolution STM image shown in the inset clearly exhibits the four-lobe pattern for each structural block at the unit cell corners. The pattern is specific for the pentamers observed at negative bias on  $(110)$  silicon and germanium surfaces [Fig. 3(d)]. Since the  $(110)$  terraces on the  $\text{Si}(47\ 35\ 7)$  surface can accommodate a single UBB in width, we assume that this surface is related to the same family of reconstructed surfaces as  $(110)$  and  $(17\ 15\ 1)$ .

In summary, we have shown that all reconstructions found on  $(110)$  silicon and germanium surfaces and their vicinals share the same building block. The atomic structure of the universal building block is proposed and it has been demonstrated that the surfaces composed of these blocks possess very low surface energies and show excellent agreement with the bias-dependent experimental

STM images. Our study concludes the long-standing debate on the atomic structures of (1 1 0) silicon and germanium surfaces, consistently describing their reconstructions on a single basis.

We would like to thank the Novosibirsk State University for providing the computational resources. This work was supported by the Russian Foundation for Basic Research (Project No. 18-02-0000025).

---

\* zhachuk@gmail.com

- [1] Y. Yamamoto, *Phys. Rev. B* **50**, 8534 (1994).
- [2] W. E. Packard and J. D. Dow, *Phys. Rev. B* **55**, 15643 (1997).
- [3] Z. Gai, R. G. Zhao, and W. S. Yang, *Phys. Rev. B* **57**, R6795 (1998).
- [4] T. An, M. Yoshimura, I. Ono, and K. Ueda, *Phys. Rev. B* **61**, 3006 (2000).
- [5] A. A. Stekolnikov, J. Furthmüller, and F. Bechstedt, *Phys. Rev. Lett.* **93**, 136104 (2004).
- [6] T. Ichikawa, *Surf. Sci.* **544**, 58 (2003).
- [7] T. Ichikawa, *Surf. Sci.* **560**, 205 (2004).
- [8] T. Ichikawa, *Surf. Sci.* **560**, 213 (2004).
- [9] K. Sakamoto, M. Setvin, K. Mawatari, P. E. J. Eriksson, K. Miki, and R. I. G. Uhrberg, *Phys. Rev. B* **79**, 045304 (2009).
- [10] M. Setvín, V. Brázdová, K. Miki, and D. R. Bowler, *Phys. Rev. B* **82**, 125421 (2010).
- [11] M. Setvín, V. Brázdová, D. R. Bowler, K. Tomatsu, K. Nakatsuji, F. Komori, and K. Miki, *Phys. Rev. B* **84**, 115317 (2011).
- [12] T. Yamasaki, K. Kato, T. Uda, T. Yamamoto, and T. Ohno, *Appl. Phys. Exp.* **9**, 035501 (2016).
- [13] N. Takeuchi, *Surf. Sci.* **494**, 21 (2001).
- [14] C. H. Mullet and S. Chiang, *Surf. Sci.* **621**, 184 (2014).
- [15] Y. Yamamoto, T. Sueyoshi, T. Sato, and M. Iwatsuki, *Surf. Sci.* **466**, 183 (2000).
- [16] Y. Ohira, M. Yoshimura, and K. Ueda, *Jap. J. Appl. Phys.* **46**, 5652 (2007).
- [17] N. D. Kim, Y. K. Kim, C.-Y. Park, H. W. Yeom, H. Koh, E. Rotenberg, and J. R. Ahn, *Phys. Rev. B* **75**, 125309 (2007).
- [18] T. Nagasawa and K. Sueoka, *J. Electrochem. Soc.* **159**, H201 (2012).
- [19] E. J. van Loenen, D. Dijkkamp, and A. J. Hoeven, *J. Microsc.* **152**, 487 (1988).
- [20] P. Bampoulis, A. Acun, L. Zhang, and H. J. W. Zandvliet, *Surf. Sci.* **626**, 1 (2014).
- [21] W. Cheng, A. Teramoto, M. Hirayama, S. Sugawa, and T. Ohmi, *Jpn. J. Appl. Phys.* **45**, 3110 (2006).
- [22] Y. Yamada, A. Girard, H. Asaoka, H. Yamamoto, and S. I. Shamoto, *Phys. Rev. B* **76**, 153309 (2007).
- [23] N. K. Lewis, N. B. Clayburn, E. Brunkow, T. J. Gay, Y. Lassailly, J. Fujii, I. Vobornik, W. R. Flavell, and E. A. Seddon, *Phys. Rev. B* **95**, 205306 (2017).
- [24] N. S. Maslova, A. I. Oreshkin, S. I. Oreshkin, V. I. Panov, I. V. Radchenko, and S. V. Savinov, *JETP Letters* **84**, 320 (2006).
- [25] I. H. Hong, Y. C. Liao, and Y. F. Tsai, *Appl. Phys. Exp.* **4**, 115003 (2011).
- [26] I. H. Hong, Y. F. Tsai, and T. M. Chen, *Appl. Phys. Lett.* **98**, 193118 (2011).
- [27] S. M. Hus and H. H. Weitering, *Appl. Phys. Lett.* **103**, 073101 (2013).
- [28] T. Watanabe, Y. Yamada, M. Sasaki, S. Sakai, and Y. Yamauchi, *Surf. Sci.* **653**, L71 (2016).
- [29] C. J. G. I. H. Hong, *Carbon* **107**, 925 (2016).
- [30] T. Ichikawa, T. Sueyoshi, T. Sato, M. Iwatsuki, F. Udagawa, and I. Sumita, *Solid State Commun.* **93**, 541 (1995).
- [31] E. A. Wood, *J. Appl. Phys.* **35**, 1306 (1964).
- [32] A. A. Stekolnikov, J. Furthmüller, and F. Bechstedt, *Phys. Rev. B* **70**, 045305 (2004).
- [33] B. Olshanetsky, S. Repinsky, and A. Shklyaev, *Surf. Sci.* **64**, 224 (1977).
- [34] Y. Yamamoto, T. Sueyoshi, T. Sato, and M. Iwatsuki, *J. Appl. Phys.* **75**, 2421 (1994).
- [35] A. I. Shkrebtii, C. M. Bertoni, R. D. Sole, and B. A. Nesterenko, *Surf. Sci.* **239**, 227 (1990).
- [36] N. Troullier and J. L. Martins, *Phys. Rev. B* **43**, 1993 (1991).
- [37] J. M. Soler, E. Artacho, J. D. Gale, A. García, J. Junquera, P. Ordejón, and D. Sánchez-Portal, *J. Phys.: Condens. Matter* **14**, 2745 (2002).
- [38] J. P. Perdew and Y. Wang, *Phys. Rev. B* **45**, 13244 (1992).
- [39] R. Zhachuk, J. Coutinho, A. Dolbak, V. Cherepanov, and B. Voigtländer, *Phys. Rev. B* **96**, 085401 (2017).
- [40] H. J. Monkhorst and J. D. Pack, *Phys. Rev. B* **13**, 5188 (1976).
- [41] J. Tersoff and D. R. Hamann, *Phys. Rev. Lett.* **50**, 1998 (1983).
- [42] W. Kohn and L. J. Sham, *Phys. Rev.* **140**, A1133 (1965).
- [43] R. Zhachuk, J. Coutinho, and K. Palotás, *J. Chem. Phys.* **149**, 204702 (2018).
- [44] I. Horcas, R. Fernández, J. M. Gómez-Rodríguez, J. Colchero, J. Gómez-Herrero, and A. M. Baro, *Rev. Sci. Instrum.* **78**, 013705 (2007).
- [45] J. Dąbrowski, H.-J. Müssig, and G. Wolff, *Phys. Rev. Lett.* **73**, 1660 (1994).
- [46] R. Zhachuk and S. Teys, *Phys. Rev. B* **95**, 041412(R) (2017).
- [47] K. Sakamoto, M. Setvin, K. Mawatari, P. E. J. Eriksson, K. Miki, and R. I. G. Uhrberg, *Phys. Rev. B* **79**, 045304 (2009).
- [48] R. Zhachuk and J. Coutinho, *JETP Lett.* **106**, 346 (2017).
- [49] R. Zhachuk and J. Coutinho, *JETP* **155**, 103 (2019).
- [50] J. P. Perdew, K. Burke, and M. Ernzerhof, *Phys. Rev. Lett.* **77**, 3865 (1996).
- [51] M. Setvín, Private communication.
- [52] D. Zhao and D. Haneman, *Surf. Sci.* **418**, 132 (1998).
- [53] Y.-N. Yang and E. D. Williams, *Phys. Rev. Lett.* **72**, 1862 (1994).
- [54] B. Z. Olshanetsky and A. A. Shklyaev, *Surf. Sci.* **82**, 445 (1979).